Supplementary Information

Nanostructured Amalgams with Tuneable Silver-Mercury Bonding Sites for Selective Electroreduction of Carbon Dioxide into Formate and Carbon Monoxide

Wanfeng Yang, Sheng Chen, Wenhao Ren, Yong Zhao, Xianjue Chen, Chen Jia, Junnan Liu, Chuan Zhao*

School of Chemistry, The University of New South Wales, Sydney, New South Wales 2052, Australia

*Corresponding author. Email: chuan.zhao@unsw.edu.au

Table S1 Atomic ratios of Ag and Hg in five np-Hg-Ag amalgams based on the quantification of EDX spectra.

Samples	Ag/Hg atomic ratio
$Ag_{100}Hg_0$	100:0
$Ag_{91}Hg_9$	93.47:6.53
$Ag_{83}Hg_{17}$	89.15:10.85
$Ag_{70}Hg_{30}$	77.20:22.80
$Ag_{60}Hg_{40}$	62.16:37.84

Table S2 Atomic ratios of Ag and Hg in five np-Hg-Ag amalgams based on the quantification of ICP-MS analysis.

Samples	Ag/Hg atomic ratio
$Ag_{100}Hg_0$	100:0
$Ag_{91}Hg_9$	93.4:6.6
$Ag_{83}Hg_{17}$	86.8:13.2
$Ag_{70}Hg_{30}$	78.1:21.9
$Ag_{60}Hg_{40}$	69.4:30.6

Table S3 Calculated results of the crystal structures and phase fractions of np-Ag-Hg amalgams based on the refinement of XRD.

Samples	(111) peak position (2θ/°)	Lattice parameters (Å)			Phase fraction (%)	
		a	b	c	Ag(Hg)	$Ag_{1.1}Hg_{0.9}$
$Ag_{100}Hg_0$	38.3	4.08867	4.08867	4.08867	/	/
$Ag_{91}Hg_9$	38.1	4.1077	4.1077	4.1077	100	0
$Ag_{83}Hg_{17}$	38.0	4.1229	4.1229	4.1229	93.9	6.1
$Ag_{70}Hg_{30}$	37.7	4.157	4.157	4.157	81.9	18.1
$Ag_{60}Hg_{40}$	37.5	4.178	4.178	4.178	83.7	16.3

Table S4 Summary of various bifunctional electrocatalysts for CO_2 reduction to formate or CO.

Catalysts	Electrolyte	Formate			CO			References
		E/V vs. RHE	FE %	*j* mA cm^{-2}	*E/V* vs. RHE	FE %	*j* mA cm^{-2}	
Ag-Hg amalgam	0.5 M $KHCO_3$	-0.9	85	5.1	-0.7	58	0.4	This work
Cu-In alloy	0.1 M $KHCO_3$	-1	62	0.73	-0.9	35	0.46	S1
Ligand-modified Pd	0.5 M $KHCO_3$	-0.57	82	1.72	-0.47	27	0.2	S2
OD-Cu	0.1 M $KHCO_3$	-0.7	36	~0.6	-0.5	43	~0.26	S3
C-Cu/SnO_2	0.5 M $KHCO_3$	-0.9	85	NA*	-0.7	93	NA	S4
Ag-Sn alloy	0.5 M $NaHCO_3$	-0.8	80	16	-0.8	18	NA	S5
$CuInO_2$	0.1 M $KHCO_3$	-0.8	70	1.4	-0.8	10	0.2	S6
Ag-In alloy	0.1 M $KHCO_3$	-1.2	90	NA	-0.8	20	NA	S7

*: Not available

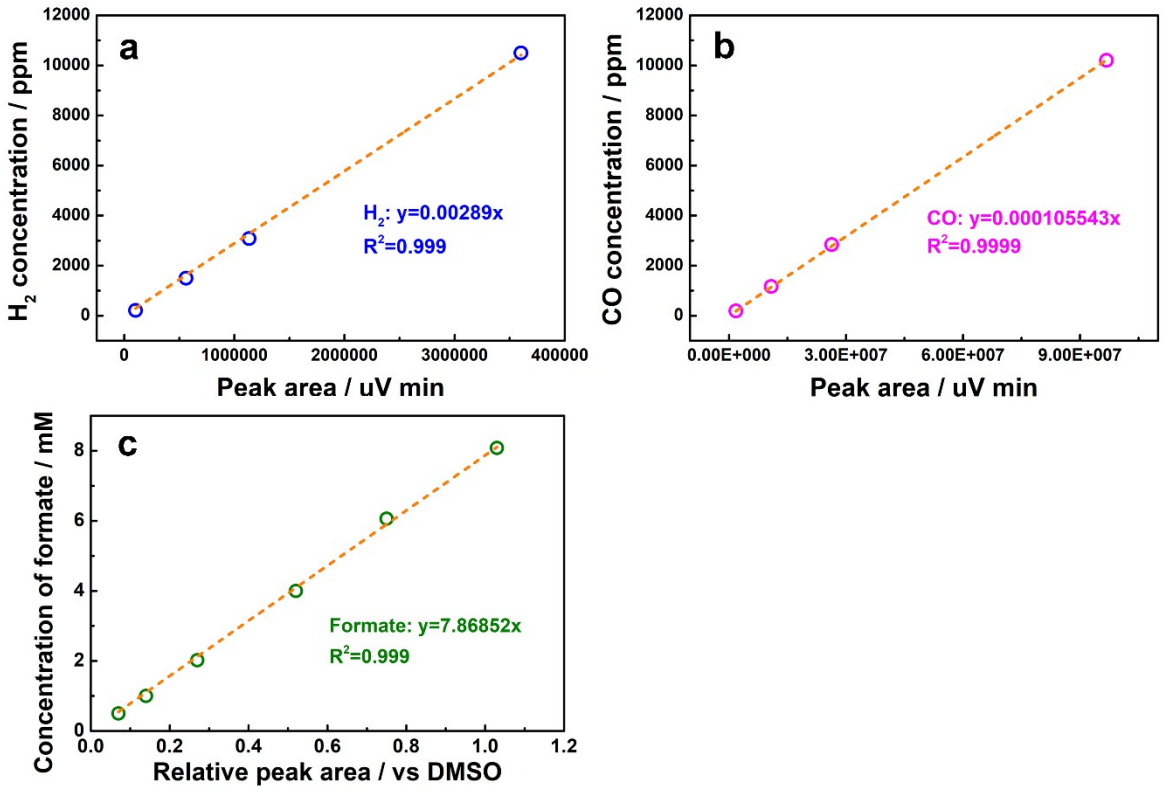

Figure S1 (a) The linear relationship between H_2 concentration and the corresponding peak area, (b) the linear relationship between the CO concentration and the corresponding peak area, (c) the linear relationship between formate concentration and the corresponding relative area vs. DMSO.

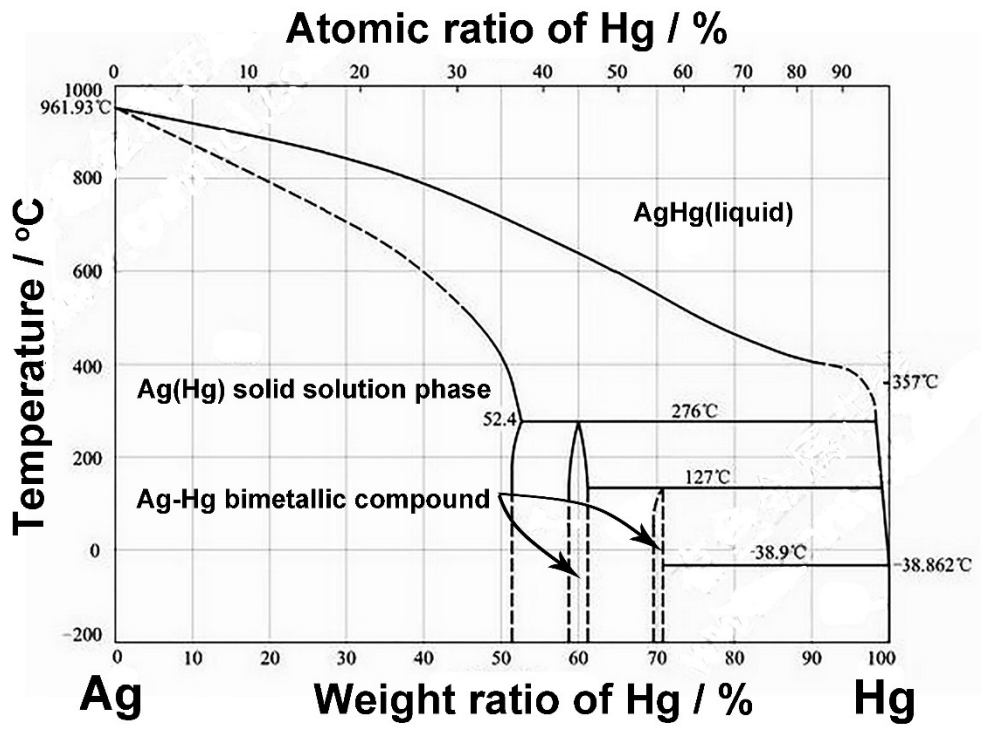

Figure S2 Ag-Hg phase diagram.[S8]

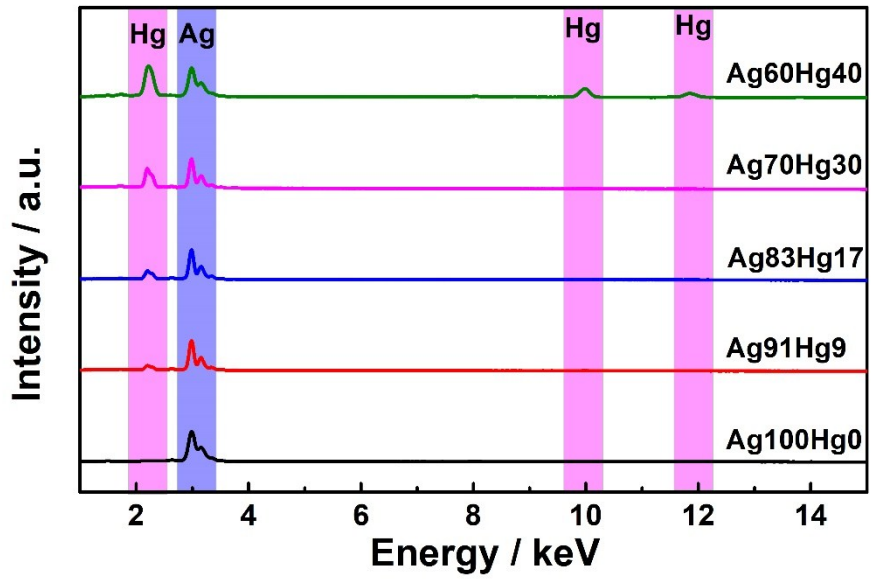

Figure S3 EDX patterns of (a)$Ag_{100}Hg_0$, (b)$Ag_{91}Hg_9$, (c)$Ag_{83}Hg_{17}$, (d)$Ag_{70}Hg_{30}$, and (e)$Ag_{60}Hg_{40}$.

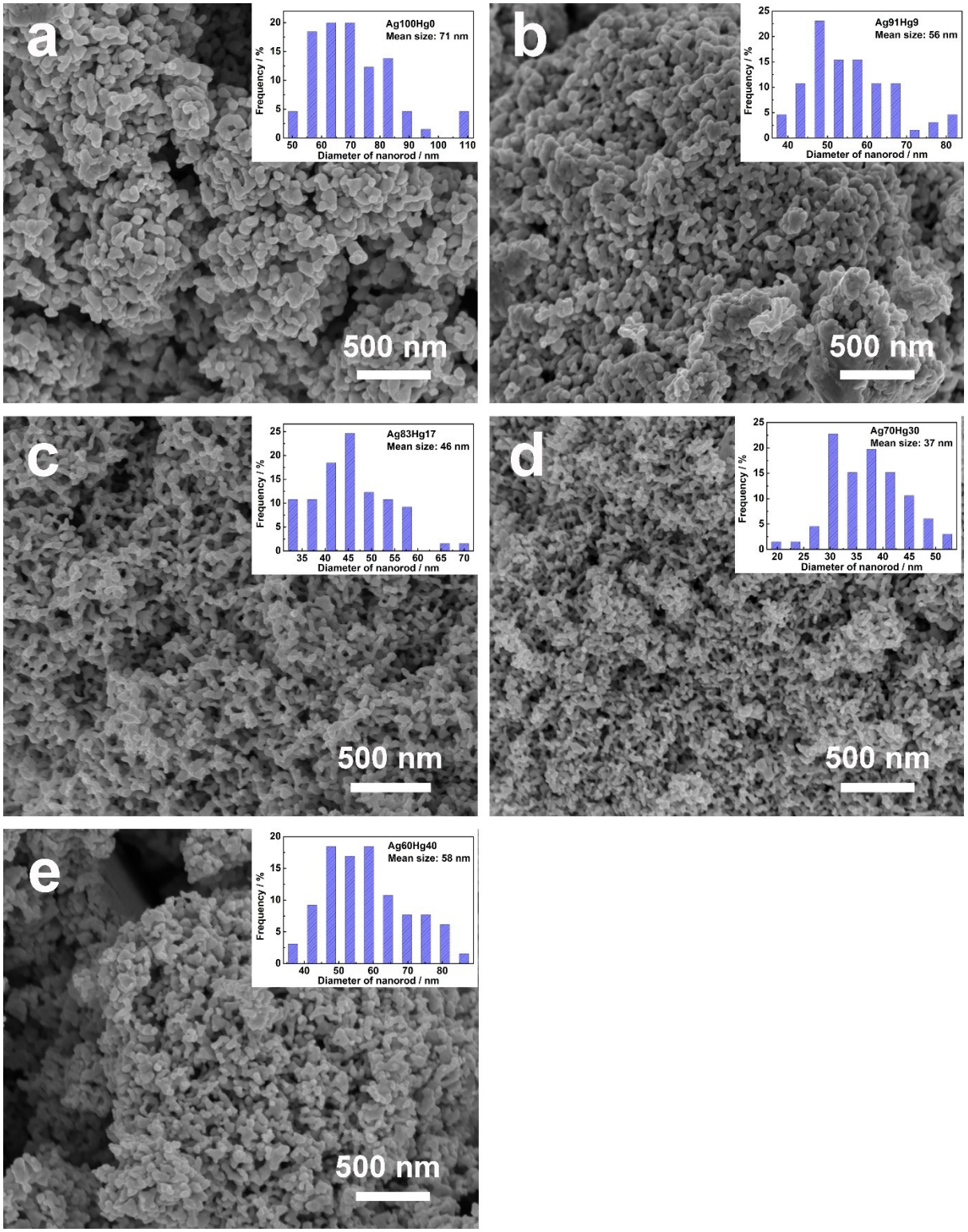

Figure S4 SEM images and diameter of nanorod distributions of (a)$Ag_{100}Hg_0$, (b)$Ag_{91}Hg_9$, (c)$Ag_{83}Hg_{17}$, (d)$Ag_{70}Hg_{30}$, and (e)$Ag_{60}Hg_{40}$.

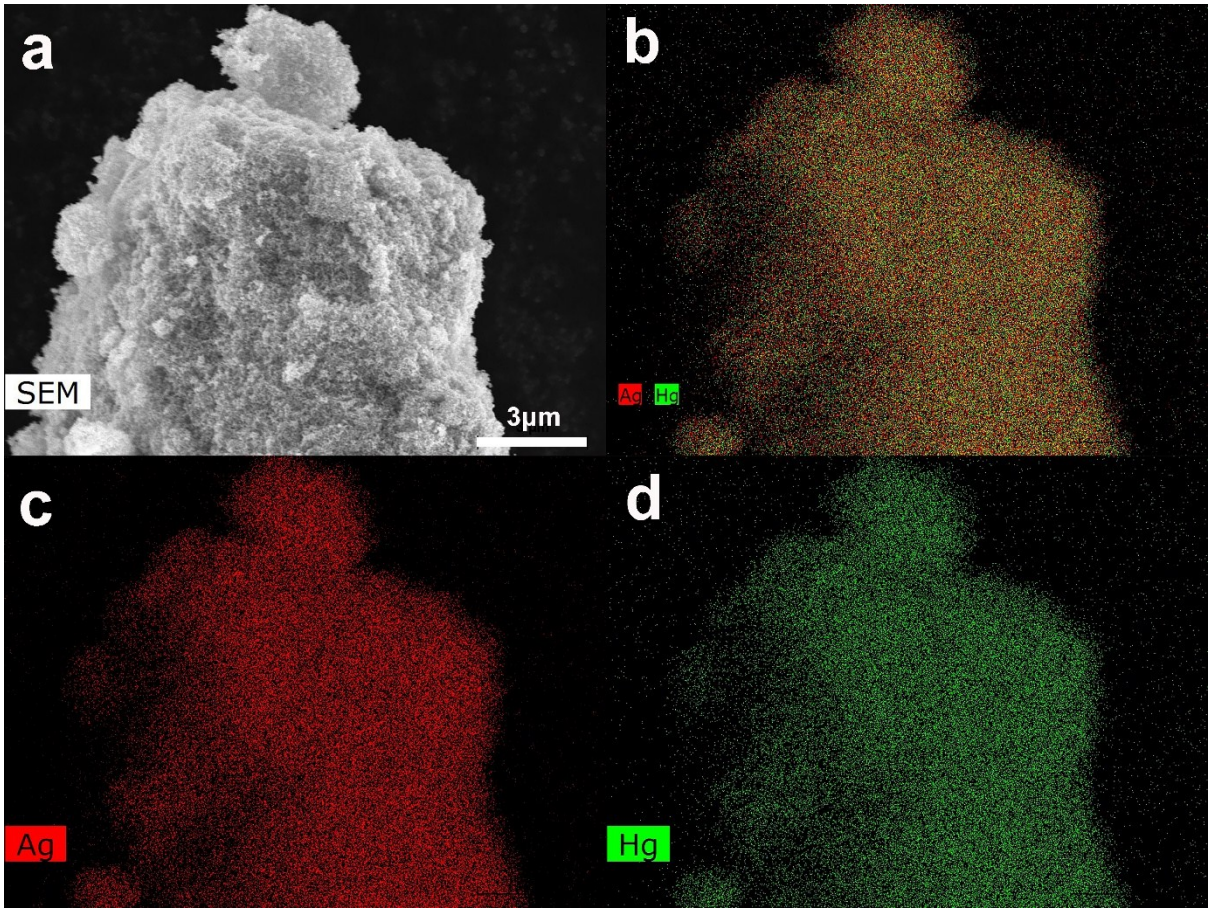

Figure S5 (a) SEM image, (b-d) the corresponding EDX mapping results, including (b) distributions of Ag and Hg mixture, (c) separated Ag distributions and (d) separated Hg distributions of $Ag_{70}Hg_{30}$.

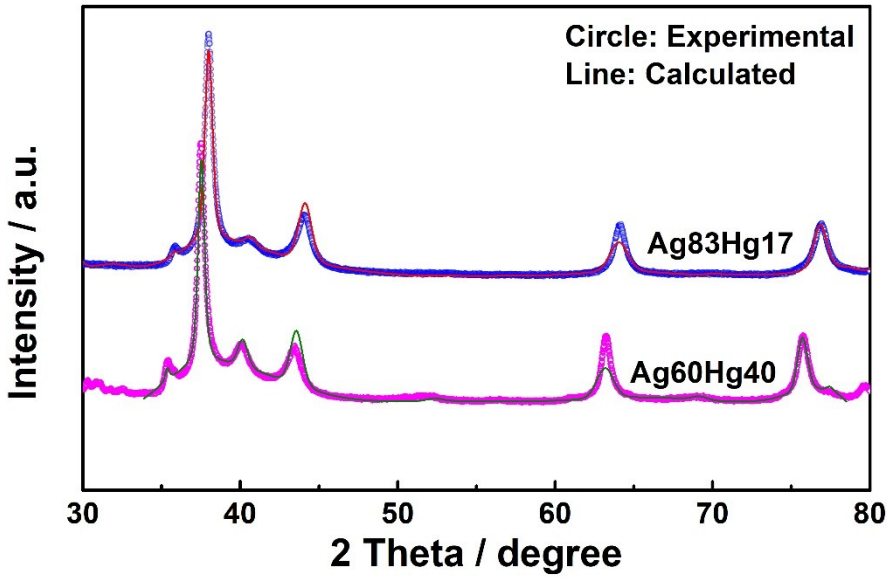

Figure S6 XRD patterns and the corresponding Rietveld refinements of $Ag_{83}Hg_{17}$ and $Ag_{60}Hg_{40}$.

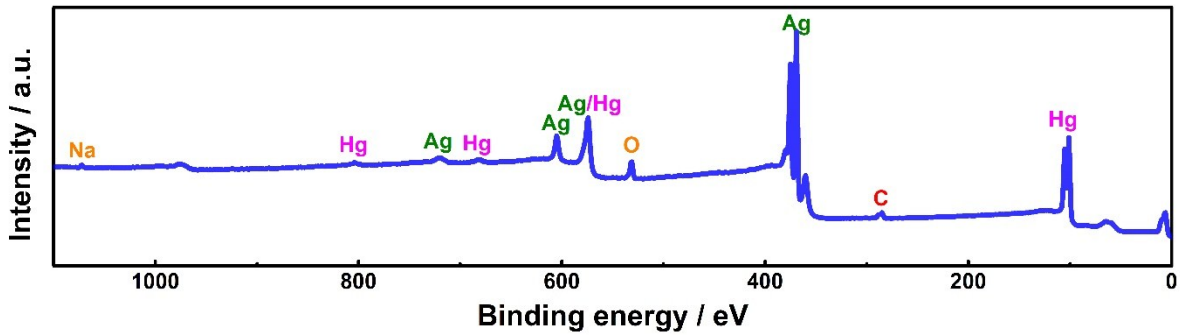

Figure S7 Full XPS spectrum of for $Ag_{70}Hg_{30}$. Carbon originates from the carbon substrate, and oxygen is from the slight surface oxidation, and sodium comes from precursors during the synthesis process.

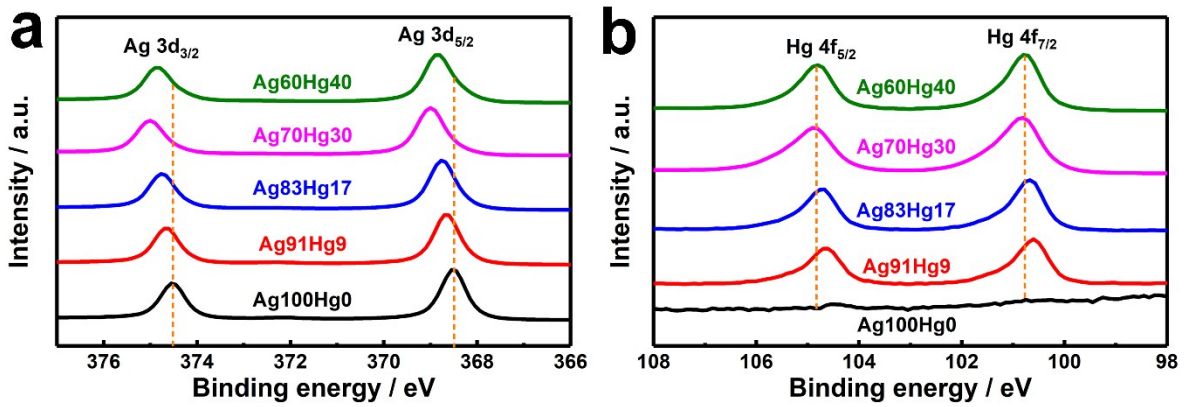

Figure S8 XPS spectra Ag3d and Hg4f peaks for $Ag_{100}Hg_0$, $Ag_{91}Hg_9$, $Ag_{83}Hg_{17}$, $Ag_{70}Hg_{30}$ and $Ag_{60}Hg_{40}$.

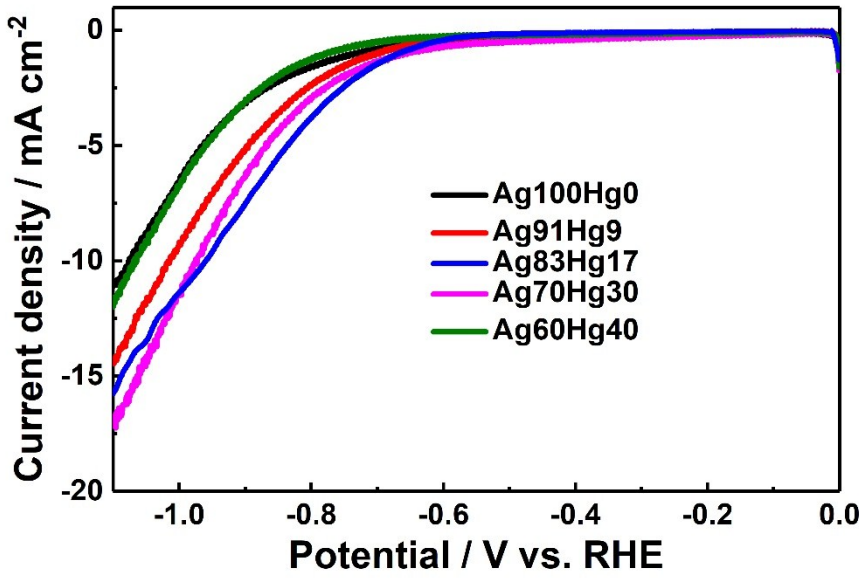

Figure S9 LSV plots in CO_2-saturated 0.5 M $KHCO_3$ aqueous solution at a scan rate of 20 mV s^{-1} for np-Ag-Hg amalgams including $Ag_{100}Hg_0$, $Ag_{91}Hg_9$, $Ag_{83}Hg_{17}$, $Ag_{70}Hg_{30}$ and $Ag_{60}Hg_{40}$.

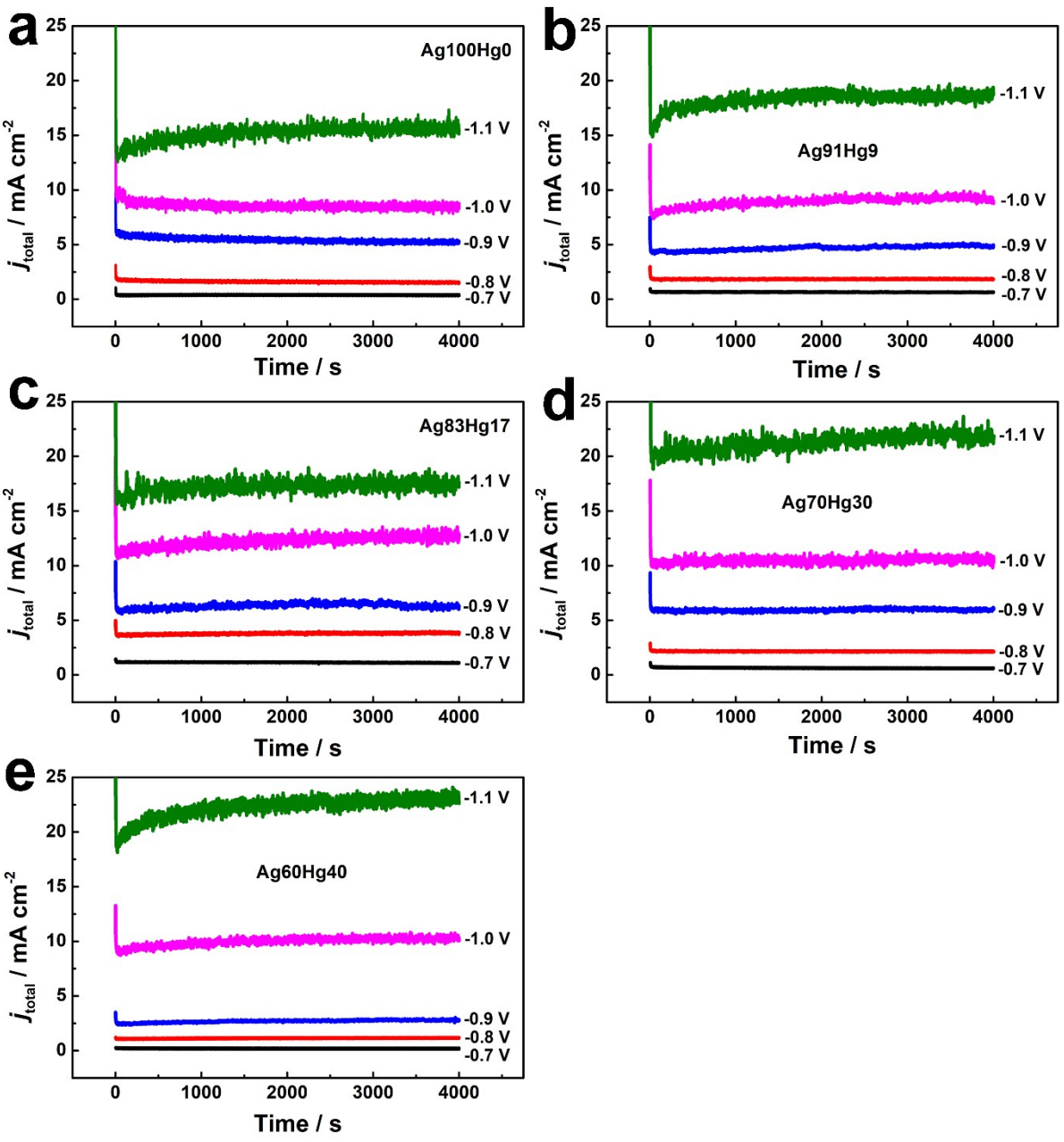

Figure S10 Representative CO_2 electroreduction curves at various potentials in CO_2-saturated 0.5 M $KHCO_3$ solution for np-Ag-Hg amalgams including (a) $Ag_{100}Hg_0$, (b) $Ag_{91}Hg_9$, (c) $Ag_{83}Hg_{17}$, (d) $Ag_{70}Hg_{30}$ and (e) $Ag_{60}Hg_{40}$.

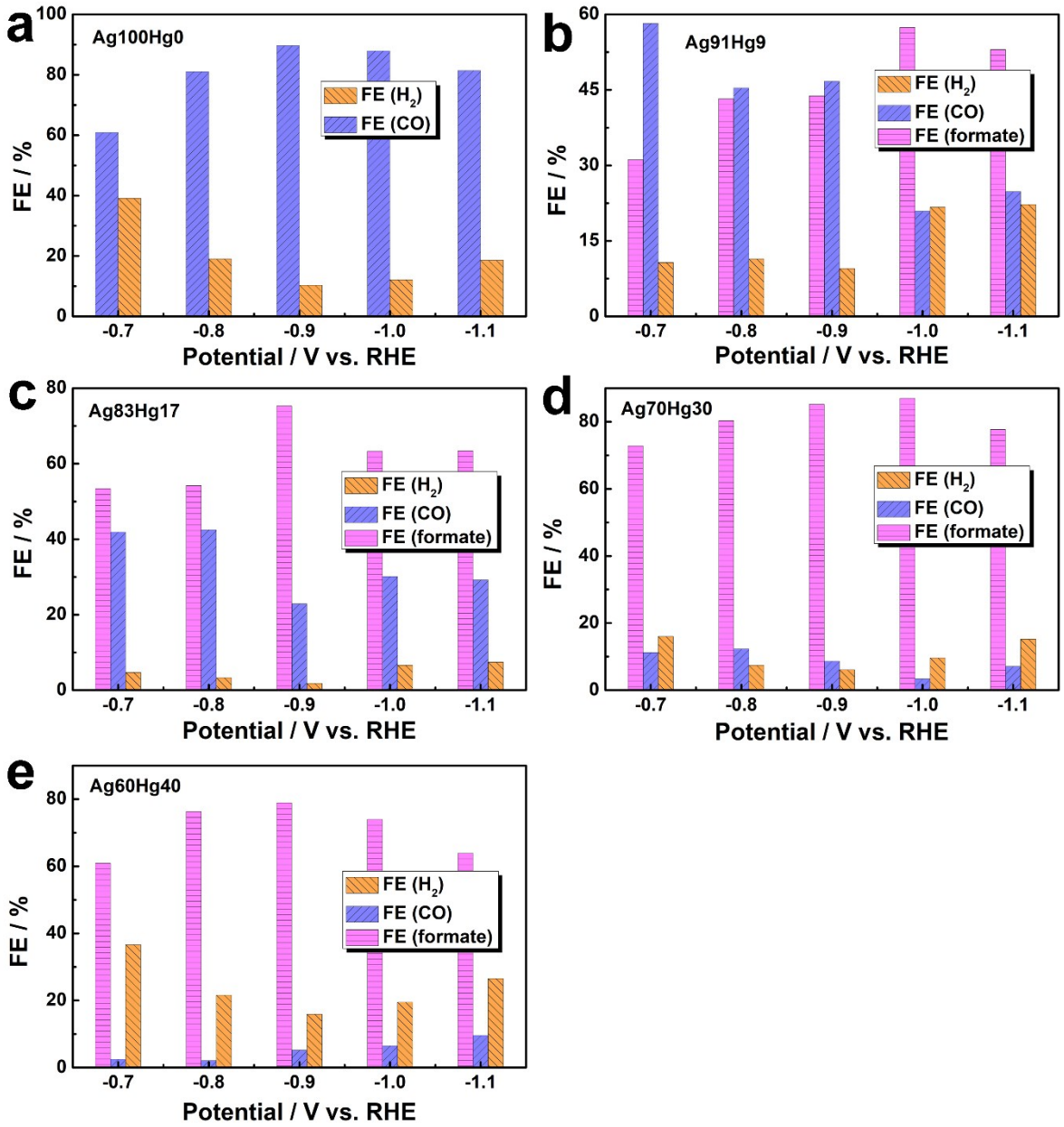

Figure S11 FEs of H_2, CO and formate at various potentials in CO_2-saturated 0.5 M $KHCO_3$ solution for np-Ag-Hg amalgams including (a) $Ag_{100}Hg_0$, (b) $Ag_{91}Hg_9$, (c) $Ag_{83}Hg_{17}$, (d) $Ag_{70}Hg_{30}$ and (e) $Ag_{60}Hg_{40}$.

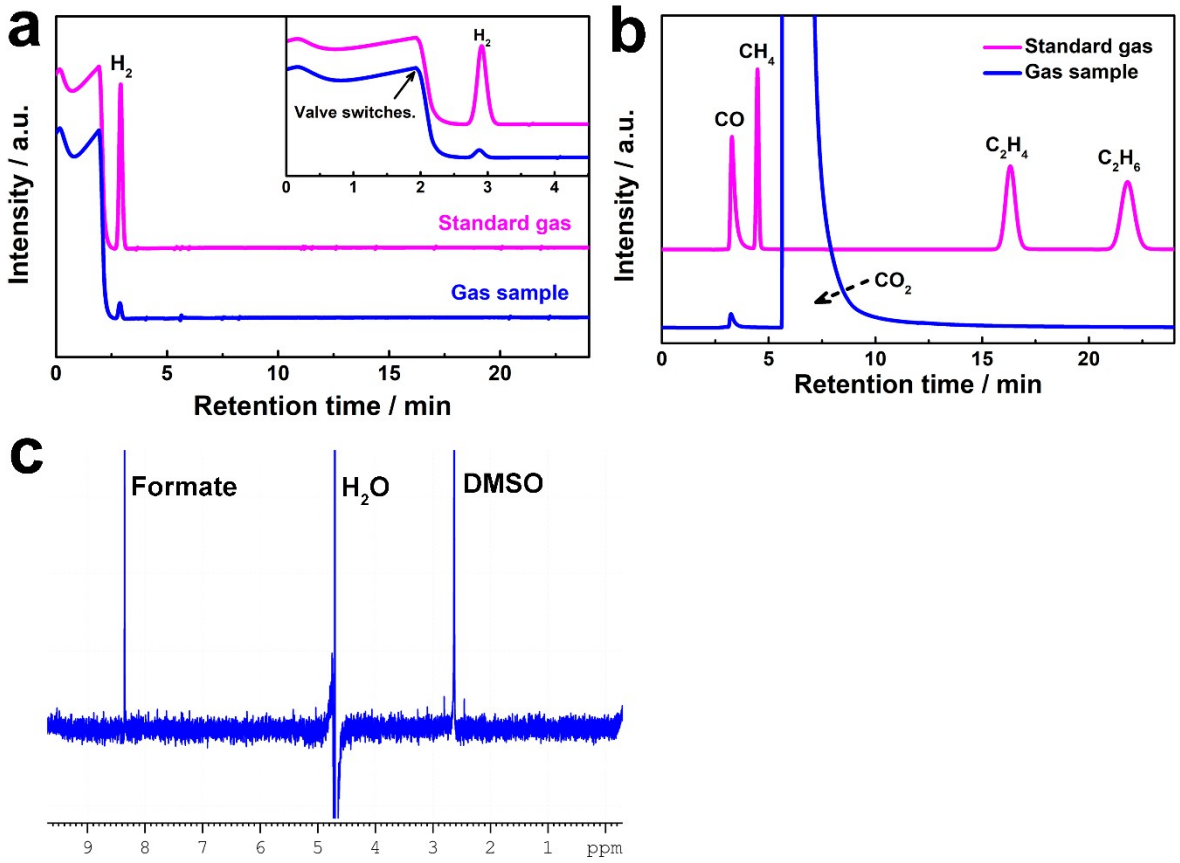

Figure S12 Selected GC spectra including (a) TCD signals, and (b) FID signals of the gas products collected at -0.9 V vs. RHE on $Ag_{70}Hg_{30}$, in comparison to the standard gas (H_2 3080 ppm, CO 1170 ppm, CH_4 964 ppm, C_2H_4: 1030 ppm, C_2H_6 970 ppm in N_2 as the balance gas). (c) Selected NMR spectrum of the liquid product collected at -0.9 V vs. RHE with chronoamperometric electrolysis of 4000 s.

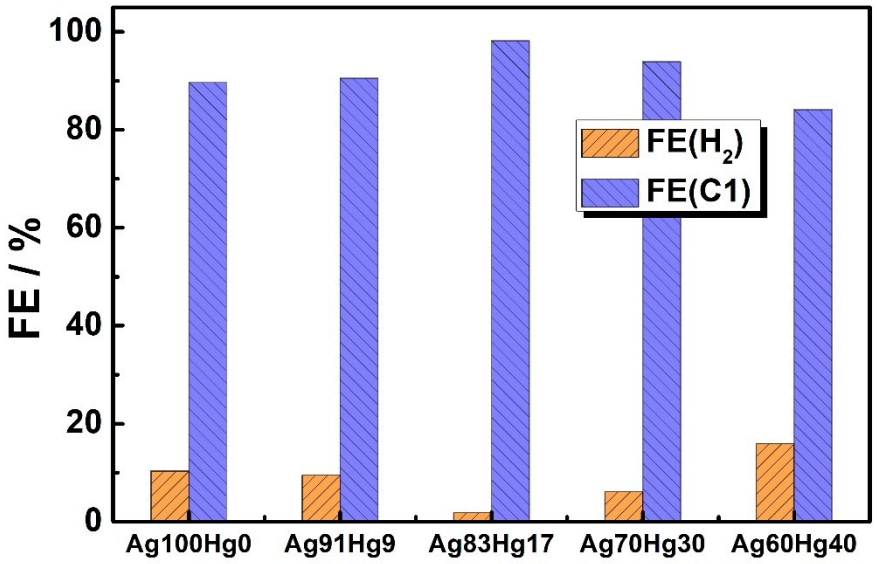

Figure S13 Electrochemical CO_2 reduction activities of np-Ag-Hg amalgams evaluated by FEs of CRR and HER at -0.9 V vs. RHE.

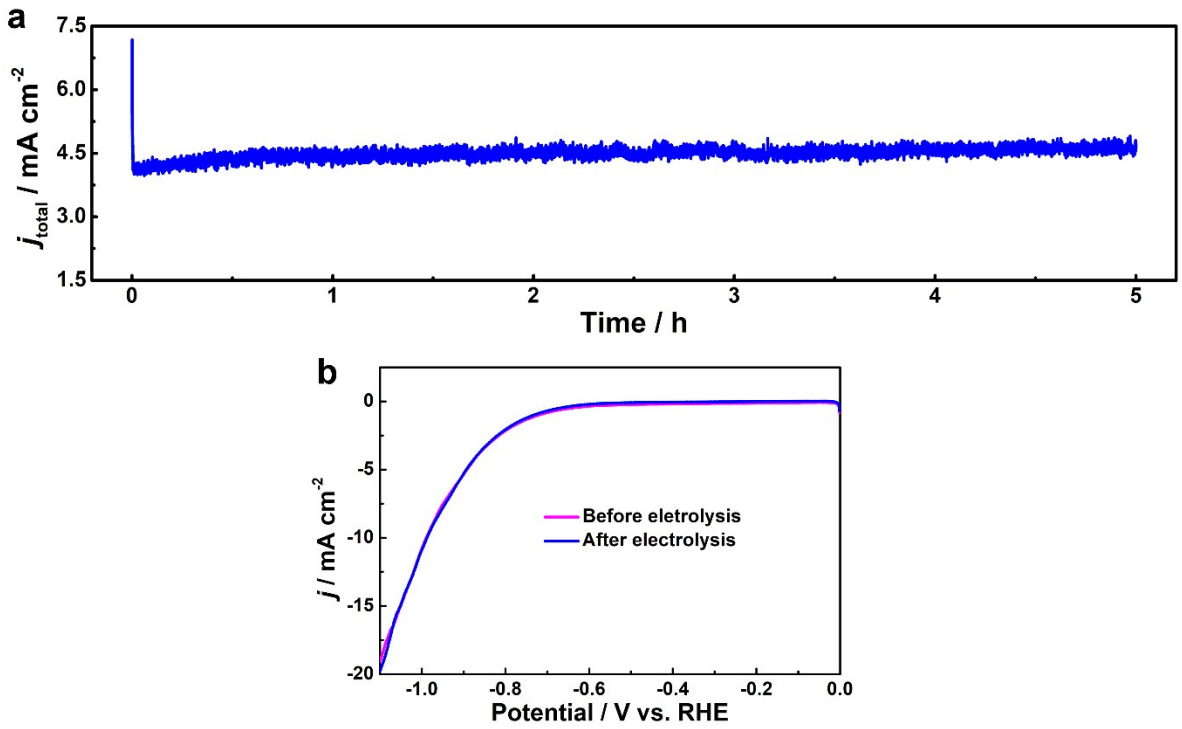

Figure S14 (a) Chronoamperometric electrolysis on $Ag_{70}Hg_{30}$ catalyst at -0.9 V vs. RHE for 5 h. (b) LSV curves on $Ag_{70}Hg_{30}$ catalyst before and after chronoamperometric electrolysis at -0.9 V vs. RHE for 5 h.

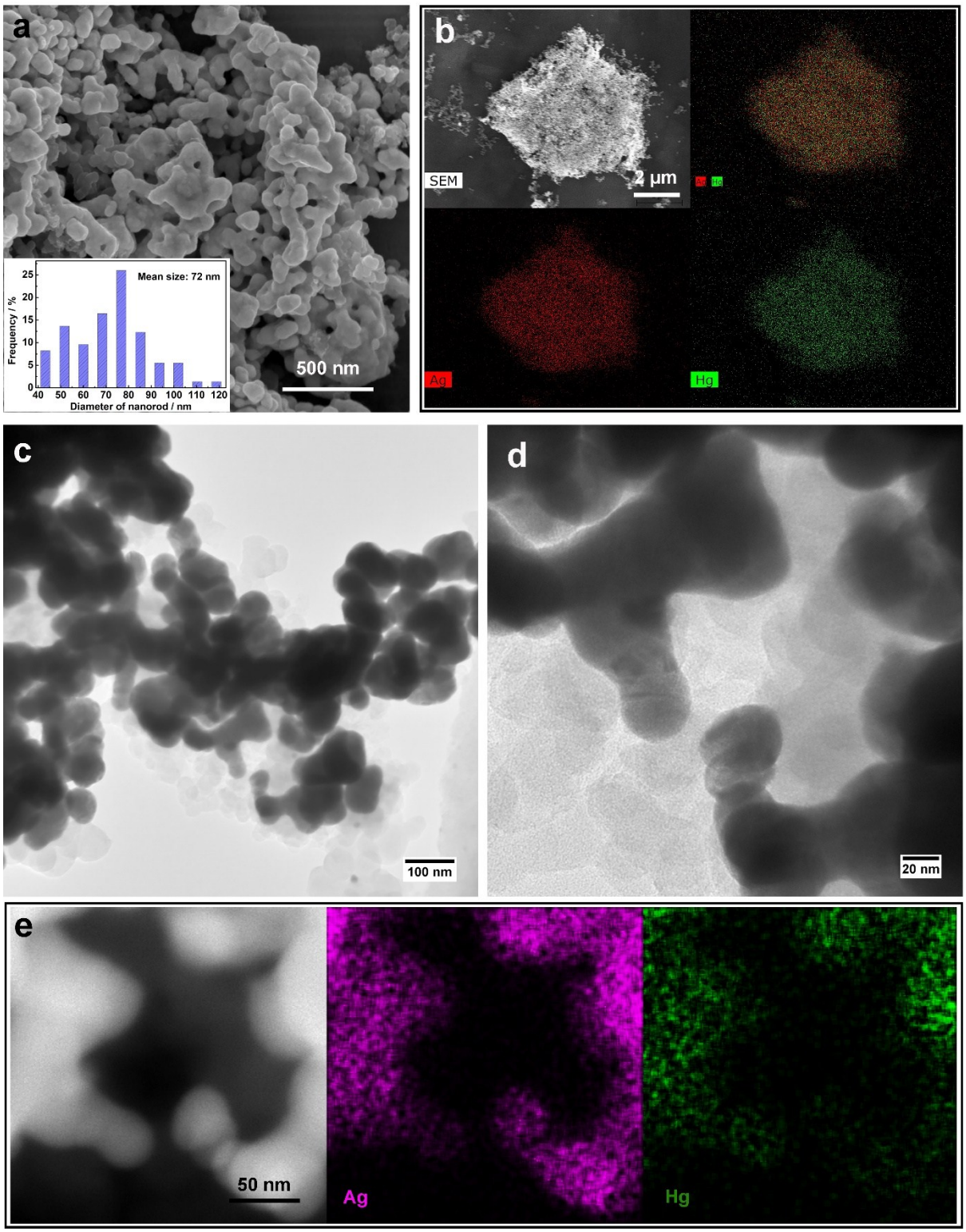

Figure S15 (a) SEM image, (b) SEM element maps, (c, d) TEM images, and (e) TEM element maps of the $Ag_{70}Hg_{30}$ after chronoamperometric electrolysis at -0.9 V vs. RHE for 5 h.

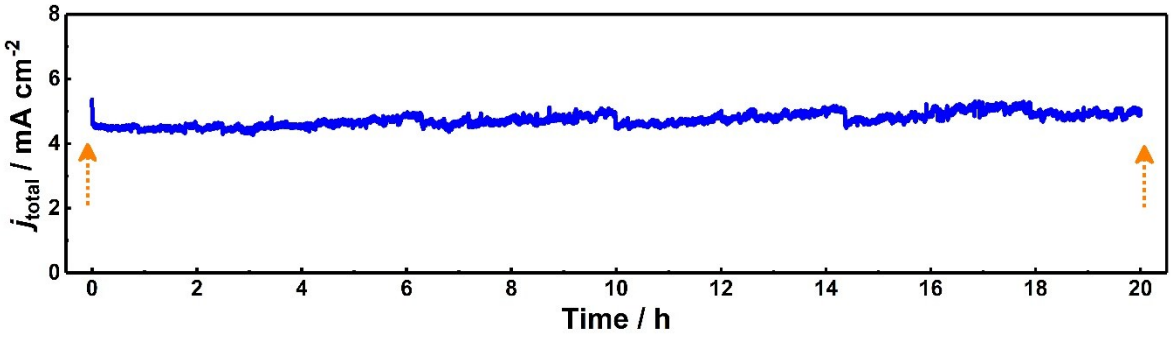

Figure S16 Chronoamperometric electrolysis on $Ag_{70}Hg_{30}$ catalyst at -0.9 V vs. RHE for 20 h in CO_2-saturated 0.5 M $KHCO_3$. The concentration of Hg^{2+} in the electrolyte before and after electrolysis was 0.024 µg l^{-1} and 0.925 µg l^{-1} respectively, which was quantified by using ICP-MS. Since the World Health Organization recommends 6 µg l^{-1} as the acceptable level of Hg^{2+} in drinking water,[S9] the Ag-Hg amalgams are stable and robust enough as the catalysts for CO_2 reduction without water pollution. Besides, around 134 µg Hg (calculated based on 0.3 mg of $Ag_{70}Hg_{30}$ per electrode with 30 at. % Hg) was used for one electrode while 0.02775 µg Hg^{2+} (calculated based on 30 ml electrolyte) was detected. This suggests that only 0.02% Hg was dissolved from the $Ag_{70}Hg_{30}$ catalyst during the electrolysis, further confirming the stability of Ag-Hg amalgams.

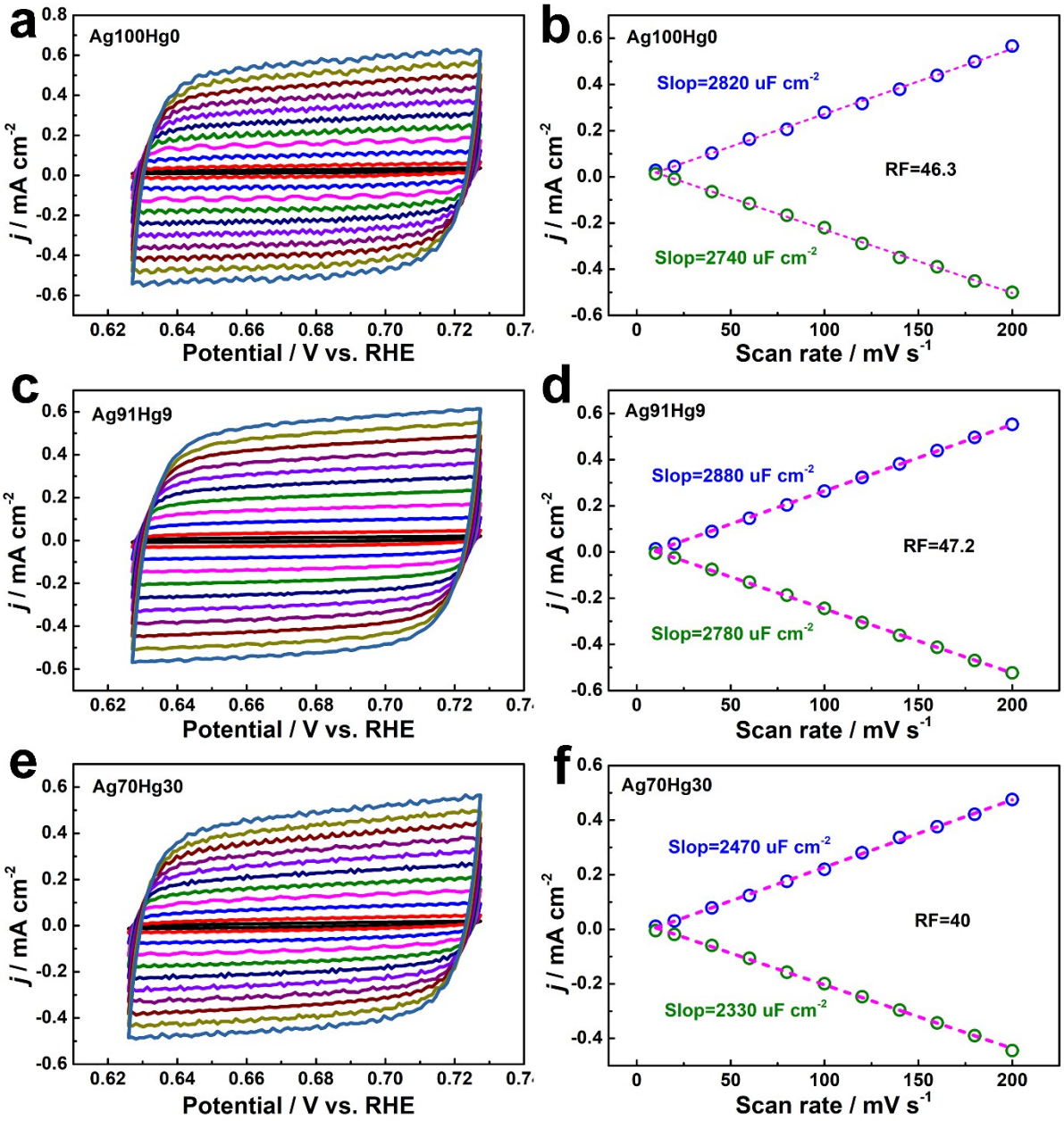

Figure S17 Electrochemical capacitance measurements to determine the ECSA of electrodes. (a, c, e) CVs measured at different scan rates and (b, d, f) the measured capacitive currents plotted as a function of scan rate of $Ag_{100}Hg_0$, $Ag_{91}Hg_9$ and $Ag_{70}Hg_{30}$, respectively.

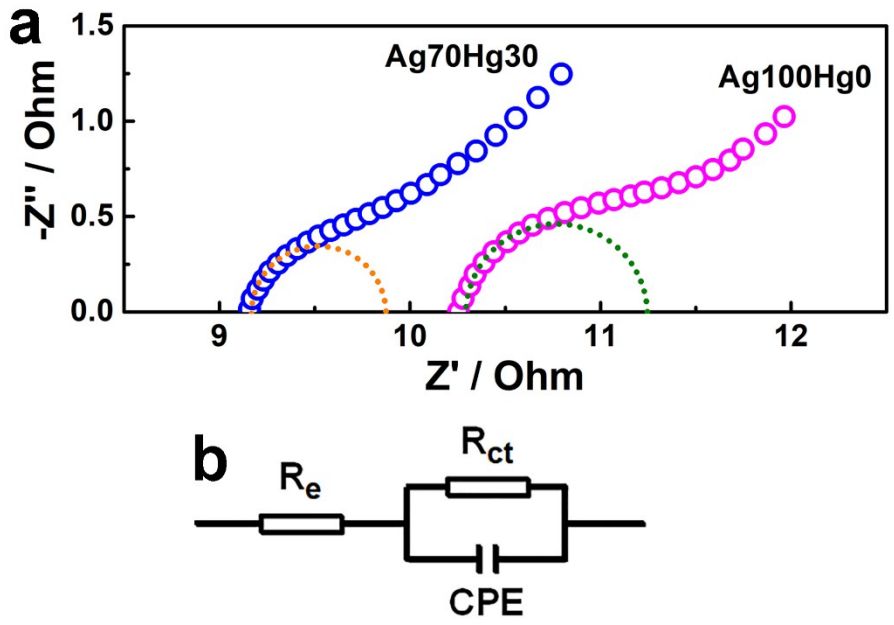

Figure S18 (a) Nyquist plots of $Ag_{70}Hg_{30}$ and $Ag_{100}Hg_{0}$ catalysts at -0.9 V vs. RHE over the frequency range of 100 Hz-100 kHz. (b) Equivalent electrical circuit corresponding to the Nyquist plots.

References

S1 Z. B. Hoffman, T. S. Gray, K. B. Moraveck, T. B. Gunnoe and G. Zangari, *ACS Catal.*, 2017, **7**, 5381.

S2 Z. Cao, J. S. Derrick, J. Xu, R. Gao, M. Gong, E. M. Nichols, P. T. Smith, X. Liu, X. Wen and C. Copéret, *Angew. Chem.*, 2018, **130**, 5075.

S3 S. Rasul, D. H. Anjum, A. Jedidi, Y. Minenkov, L. Cavallo and K. Takanabe, *Angew. Chem. Int. Ed.*, 2015, **54**, 2146.

S4 Q. Li, J. Fu, W. Zhu, Z. Chen, B. Shen, L. Wu, Z. Xi, T. Wang, G. Lu and J.-j. Zhu, *J. Am. Chem. Soc.*, 2017, **139**, 4290.

S5 W. Luc, C. Collins, S. Wang, H. Xin, K. He, Y. Kang and F. Jiao, *J. Am. Chem. Soc.*, 2017, **139**, 1885.

S6 A. Jedidi, S. Rasul, D. Masih, L. Cavallo and K. Takanabe, *J. Mater. Chem. A*, 2015, **3**, 19085.

S7 G. O. Larrazábal, A. J. Martín, S. Mitchell, R. Hauert and J. Pérez-Ramírez, *J. Catal.*, 2016, **343**, 266.

S8 M. Baren, *J. Phase Equilib.*, 1996, **17**, 122.

S9 World Health Organization (WHO), *Guideline for drinking water quality*, Geneva (Switzerland), 4th edn, 2011.